Uncertainties of GPM DPR Rain Estimates Caused by DSD Parameterizations

LIANG LIAO

Goddard Earth Sciences and Technology Center/Morgan State University, Greenbelt, Maryland

ROBERT MENEGHINI

NASA Goddard Space Flight Center, Greenbelt, Maryland

ALI TOKAY

Joint Center for Earth Systems Technology, University of Maryland, Baltimore County, Baltimore, and NASA Goddard Space Flight Center, Greenbelt, Maryland

(Manuscript received 5 December 2013, in final form 3 July 2014)

ABSTRACT

A framework based on measured raindrop size distribution (DSD) data has been developed to assess uncertainties in DSD models employed in Ku- and Ka-band dual-wavelength radar retrievals. In this study, the rain rates and attenuation coefficients from DSD parameters derived by dual-wavelength algorithms are compared with those directly obtained from measured DSD spectra. The impact of the DSD gamma parameterizations on rain estimation from the Global Precipitation Measurement mission (GPM) Dual-Frequency Precipitation Radar (DPR) is examined for the cases of a fixed shape factor μ as well as for a constrained μ—that is, a μ–Λ relation (a relationship between the shape parameter and slope parameter Λ of the gamma DSD)—by using 11 Particle Size and Velocity (Parsivel) disdrometer measurements with a total number of about 50 000 one-minute spectra that were collected during the Iowa Flood Studies (IFloodS) experiment. It is found that the DPR-like dual-wavelength techniques provide fairly accurate estimates of rain rate and attenuation if a fixed-μ gamma DSD model is used, with the value of μ ranging from 3 to 6. Comparison of the results reveals that the retrieval errors from the μ–Λ relations are generally small, with biases of less than $\pm 10\%$, and are comparable to the results from a fixed-μ gamma model with μ equal to 3 and 6. The DSD evaluation procedure is also applied to retrievals in which a lognormal DSD model is used.

1. Introduction

The Ku- and Ka-band Dual-Frequency Precipitation Radar (DPR) is one of the instruments aboard the Global Precipitation Measurement mission *Core Observatory* (GPM) satellite launched on 27 February 2014 (Hou et al. 2008). The DPR derives rain rate by estimating parameters of the raindrop size distribution (DSD), which is often modeled by an analytical function such as the exponential, gamma, or lognormal distribution, with two or three unknown parameters (Gorgucci et al. 2000, 2002; Bringi et al. 2002; Feingold and Levin 1986). The inability of the modeled DSD to represent actual DSD spectra, as well as intrinsic variations of DSD in time and space, leads to uncertainties in the estimates of rainfall rate obtained from the DPR. Understanding the uncertainties in rain estimation that depend on DSD parameterizations is important in evaluating the overall performance of DPR rain-retrieval algorithms. DSD parameterization models have an impact not only on the relationship between radar reflectivity and rain rate but also on attenuation corrections that are needed to compensate for the loss of the radar signal caused by precipitation.

Analysis of the uncertainties associated with the DSD model employed in the DPR rain-estimation procedure also provides insight into the selection of DSD models adopted in the Ku- and Ka-band dual-wavelength radar rain-profiling algorithms. Many studies have been carried out in an attempt to establish accurate DSD models using a wealth of disdrometer observations in various climate regimes (Schönhuber et al. 2007; Thurai et al. 2011;

Corresponding author address: Dr. Liang Liao, Goddard Earth Science Technology/MSU, Code 612, NASA Goddard Space Flight Center, Greenbelt, MD 20771.
E-mail: liang.liao-1@nasa.gov

DOI: 10.1175/JAMC-D-14-0003.1

© 2014 American Meteorological Society

Tokay et al. 2013; Williams et al. 2014). Most of these studies rely on either linear/nonlinear-regression methods or the method of moments (Smith et al. 2009). These are general approaches that attempt to minimize discrepancies between the modeled and measured DSD spectra. For dual-wavelength radar applications, an alternative approach is to assess the uncertainties in the DSD parameterization on the basis of radar-estimated rain rates (rather than those derived from DSD models). As mentioned earlier, most dual-frequency radar retrievals derive rain rate by first estimating parameters of the DSD, typically through the use of a gamma distribution. Thus, uncertainties in the DSD models employed in the radar algorithms directly affect the dual-frequency radar retrieval of rainfall rate. In this paper we evaluate these uncertainties by comparing radar-derived estimates of rain rate with those directly computed from DSD measurements.

In this study, we employ measured DSD data taken from the Iowa Flood Studies (IFloodS) to generate the radar reflectivity factors at Ku and Ka band. These radar reflectivities are then used to estimate the DSD parameters, under an assumed DSD model. Dual-frequency radar techniques usually make use of the differential frequency ratio (DFR), defined as the difference between radar reflectivities (dB) at two frequencies, as well as the radar reflectivity at the lower frequency to first infer the DSD parameters and then from them the rain rate (Meneghini et al. 1997; Mardiana et al. 2004; Liao and Meneghini 2005; Rose and Chandrasekar 2005; Seto et al. 2013). The rain rates estimated from the radar-derived DSD are compared with those that were directly obtained from the measured DSD spectra. Note that the rain rates derived from the measured DSD serve as a benchmark or truth for checking radar estimates. By this procedure, the difference between the rain rate retrieved by the radar and the directly measured rain rate can be interpreted as the uncertainty in the radar rain estimation arising from the DSD parameterization and the inherent errors in the radar retrieval method. To assess the impact of the uncertainties associated with the DSD parameterizations on attenuation corrections and the overall performance of the DPR rain-retrieval algorithms, error statistics for the rain rate, median mass diameter, and specific attenuation are presented. Because the simulated reflectivities are directly computed from the measured DSD spectra, they serve as the true or unattenuated radar reflectivity factors. The ultimate goal of this study is to evaluate the uncertainties in the DPR rain-estimation algorithms that arise from the assumed DSD model and thereby to provide guidance on the choice of DSD model that is appropriate for the DPR retrieval algorithm.

Note that, in addition to the choice of DSD parameterization, the DPR algorithm requires modeling of environmental conditions, making use of path-attenuation constraints, hydrometeor-phase identifications, and particle-scattering models while accounting for nonuniform beam filling among other considerations (Meneghini and Liao 2013; Seto et al. 2013). The focus of this study is solely on the impact of DSD parameterizations on the DPR retrieval of rainfall rate, however.

In this paper, a brief description of the dual-wavelength radar technique that is used to infer DSD parameters and rain rate is given in section 2. The DSD data used in this study are described in section 3, and the procedures used to evaluate dual-wavelength radar estimates are outlined in section 4. In section 5, comparisons of the DPR-estimated rain rates and specific attenuations with those that were directly computed from measured DSD spectra as well as relative errors of different DSD models are given, followed by remarks and a summary of the study in section 6.

2. Dual-wavelength techniques

The measured or apparent radar reflectivity factor Z_m of the hydrometeors at wavelength λ can be described as (e.g., Battan 1973)

$$Z_m = Z_e \exp\left(-2\int_0^r k\,dr\right), \tag{1}$$

where specific attenuation k and effective radar reflectivity factor Z_e are expressed by

$$Z_e = \frac{\lambda^4}{\pi^5|K_w|^2}\int_0^\infty N(D)\sigma_b(D,\lambda)\,dD \quad \text{and} \tag{2}$$

$$k = \int_0^\infty N(D)\sigma_e(D,\lambda)\,dD, \tag{3}$$

with $N(D)$ being the DSD and $\sigma_b(D, \lambda)$ and $\sigma_e(D, \lambda)$ being the backscattering and extinction cross sections, respectively, of a particle with diameter D. The dielectric factor K_w is related to the complex refractive index of water. By convention, $|K_w|^2$ is taken to be 0.93.

The gamma distribution is widely used to describe the DSD in the retrieval of the microphysical properties of hydrometeors (e.g., Ulbrich 1983). A form of the gamma size distribution of $N(D)$ is expressed as (Bringi and Chandrasekar 2001)

$$N(D) = N_w f(\mu)(D/D_m)^\mu \exp(-\Lambda D), \tag{4}$$

where N_w is a scale factor of DSD,

$$f(\mu) = \frac{6(4+\mu)^{\mu+4}}{4^4\Gamma(\mu+4)}, \quad \text{and} \tag{5}$$

$$\Lambda = (4+\mu)/D_m \tag{6}$$

and where Γ is the gamma function, μ is the shape factor, and D_m is the mass-weighted diameter of the particles, defined by

$$D_m = \frac{\int_{D_{\min}}^{D_{\max}} D^4 N(D)\, dD}{\int_{D_{\min}}^{D_{\max}} D^3 N(D)\, dD}. \tag{7}$$

Here $D_{\min}$ and $D_{\max}$ are the minimum and maximum diameters of raindrops, respectively. The radar DFR (dB), describing the difference of the radar reflectivity at two wavelengths, is defined as

$$\mathrm{DFR} = 10\log(Z_1/Z_2), \tag{8}$$

where Z_1 and Z_2 are the radar reflectivity factors at wavelengths of λ_1 and λ_2, respectively. Note that the DFR is independent of N_w. For dual-wavelength radar application, it is convenient to use N_w-normalized radar reflectivity I_b and specific attenuation I_e (i.e., $N_w = 1\,\mathrm{mm}^{-1}\,\mathrm{m}^{-3}$). Thus, we have

$$I_b(D_m,\mu,\lambda) = 10\log_{10}\left[\frac{\lambda^4}{\pi^5|K_w|^2}\int_{D_{\min}}^{D_{\max}} f(\mu)(D/D_m)^{\mu}\exp(-\Lambda D)\sigma_b(D,\lambda)\, dD\right] \quad \text{and} \tag{9}$$

$$I_e(D_m,\mu,\lambda) = 4.343\times10^{-3}\int_{D_{\min}}^{D_{\max}} f(\mu)(D/D_m)^{\mu}\exp(-\Lambda D)\sigma_e(D,\lambda)\, dD. \tag{10}$$

Note that N_w is suppressed in the above equations because it is assumed to be unity; $D_{\min}$ and $D_{\max}$ are taken at the nominal values of 0.1 and 8 mm, respectively. For arbitrary values of N_w, the integral-scattering parameters can be determined from the following equations:

$$\mathrm{DFR}(D_m,\mu) = I_b(D_m,\mu,\lambda_1) - I_b(D_m,\mu,\lambda_2), \tag{11}$$

$$Z_{\mathrm{dB}}(N_w,D_m,\mu,\lambda) = 10\log_{10}N_w + I_b(D_m,\mu,\lambda), \quad \text{and} \tag{12}$$

$$k(N_w,D_m,\mu,\lambda) = N_w I_e(D_m,\mu,\lambda), \tag{13}$$

where DFR, reflectivity factor Z_{dB}, and k are in units of decibels, reflectivity decibels (dBZ), and decibels per kilometer, respectively; I_b and I_e are precomputed on the basis of particle-scattering models and are stored in integral-scattering tables that are organized in terms of wavelength, D_m, and μ (or μ–Λ relations). From the attenuation-corrected DFR and $Z_{\mathrm{dB}}(\lambda_1)$, D_m is first solved from Eq. (11) under an assumption of μ, and then N_w is obtained from Eq. (12). Specific attenuations are easily computed from Eq. (13) if DSD parameters are known. The rain rate is computed by

$$R = 6\pi\times10^{-4}\int_{D_{\min}}^{D_{\max}} N_w f(\mu)(D/D_m)^{\mu}\exp[-(4+\mu)D/D_m]D^3V(D)\, dD, \tag{14}$$

where $V(D)$ is raindrop fall velocity and is expressed as a function of the particle diameter. Note that I_b and I_e are important scattering quantities that are repeatedly used in dual-wavelength techniques to compute D_m, N_w, and the attenuation coefficients.

Figure 1 shows the results of the integral-scattering lookup table where I_b [Eq. (9)] and DFR [Eq. (11)] are plotted versus D_m and temperature for the gamma distribution of rain for the case of the GPM Ku- and Ka-band DPR. The raindrops are prescribed as oblate spheroids, and their axis ratios follow the shape–size relations reported by Thurai et al. (2007). The T-matrix method is used to compute the scattering properties of single particles (Mishchenko and Travis 1998). At a fixed μ, D_m is solely dependent on the DFR over the range in which D_m is greater than ~1 mm. The one-to-one relation between D_m and DFR provides a means to estimate D_m once attenuation effects have been corrected. A double root of D_m occurs for liquid water particles when the DFR is less than 0, however, with one solution from the lower branch of the DFR–D_m relation and another from the upper branch. This feature leads to an ambiguity in the estimate of D_m, but the ambiguity can be resolved to a large extent if the radar

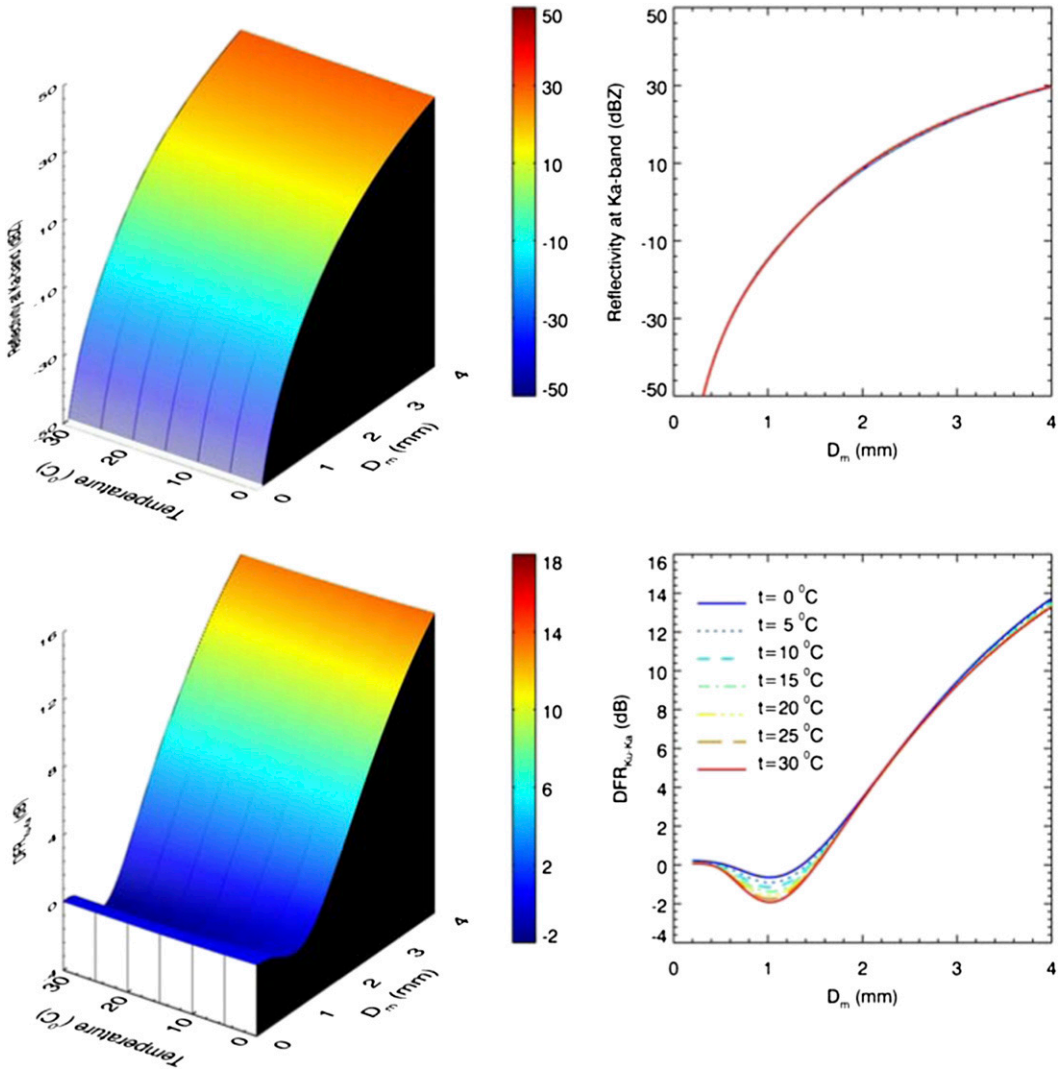

FIG. 1. Integral-scattering lookup table showing (top) the Ku-band radar reflectivity factor with $N_w = 1\,\mathrm{mm}^{-1}\,\mathrm{m}^{-3}$ as a function of D_m and temperature and (bottom) DFR vs D_m for different temperatures. For all results, a constant shape factor ($\mu = 3$) of the gamma distribution DSD model is assumed.

reflectivity is used in the selection of the proper root (Liao and Meneghini 2005).

3. DSD measurement data

The DSD data used in this study are primarily from measurements made by Particle Size and Velocity (Parsivel) disdrometers during the IFloodS field experiment from 1 May to 15 June 2013. The Parsivel disdrometers are used to measure rain DSD and fall velocities of particle sizes from 0.3 to 20 mm. During IFloodS, 14 OTT Hydromet GmbH Parsivel^2 instruments were operated at 13 different sites. The OTT Parsivel^2 is an improved version of the OTT Parsivel. The OTT Parsivel severely underestimates small drops (<0.8 mm in diameter) and overestimates large drops (>3 mm in diameter), especially in heavy rain (Tokay et al. 2013). A comparative study by Tokay et al. (2014) documented the improvement reached by the OTT Parsivel^2, showing that the issues at both ends of the spectrum are largely resolved with the new design.

At 10 of the 13 Parsivel^2 sites, Met One Instruments, Inc., tipping-bucket rain gauges were collocated with the Parsivel^2 disdrometers. Tipping-bucket gauges are often employed as a reference for event rain totals (Tokay et al. 2013, 2014). Our comparative study reveals that there is generally very good agreement between the gauges and Parsivel^2 disdrometers. Data from 11 of the 14 Parsivel^2 disdrometers were selected for this study on the basis of either the degree of accuracy with which the rain rates

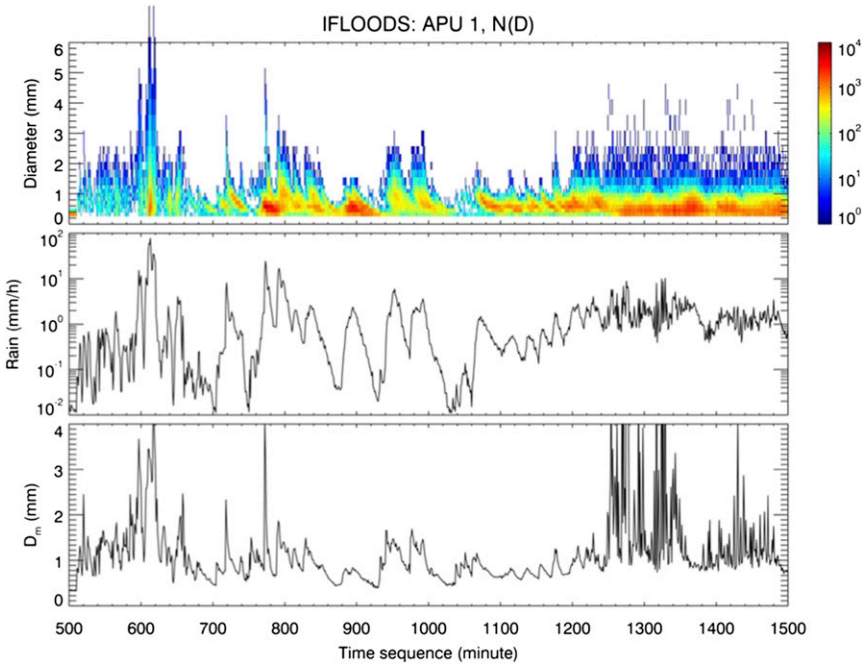

FIG. 2. Example of a time series of DSD measurements from the Parsivel disdrometer. Shown are (top) the size spectra ($\mathrm{mm^{-1}\,m^{-3}}$) and the corresponding (middle) rain rate ($\mathrm{mm\,h^{-1}}$) and (bottom) mass-weighted mean diameter D_m (mm).

inferred from disdrometer data agree with those from collocated tipping-bucket gauges or agreement of the rain rate from selected disdrometers with those from other collocated disdrometers. The criterion used was that the event rain total derived from the disdrometer data be within 10% of that obtained from the collocated rain gauge. Seven of the Parsivel[2] disdrometers meet this standard, with the majority having errors that are within 5% of the gauge values.

The disdrometer observations are stored at 1-min resolution, and the data from all units are merged into a single file. Mass-weighted particle diameter D_m can be directly computed from the DSD by Eq. (7), and rain rate R is obtained from

$$R = 6\pi \times 10^{-4} \int_{D_{\min}}^{D_{\max}} N(D) D^3 V(D)\, dD. \qquad (15)$$

Figure 2 shows an example of DSD measurements versus time taken from one of the Parsivel disdrometeors over approximately 1000 min of data. The image of the DSD spectra ($\mathrm{mm^{-1}\,m^{-1}}$), given in the top panel of Fig. 2 with the color scale on the right, is displayed in terms of particle diameter (mm) along the ordinate and time (minute) along the abscissa. The rain rate ($\mathrm{mm\,h^{-1}}$) and mass-weighted diameter computed from DSD are given in the middle and bottom panels of Fig. 2, respectively, for the same time period. Figure 3 shows the statistical mean of the DSD spectra collected by all 11 Parsivel disdrometers during the 6-week field campaign. On the abscissa are displayed the corresponding values of rain rate and D_m. It is evident that the DSD spectra are broadened as the rain rate and D_m increase, implying that $D_{\max}$ is closely related to rain rate and D_m (Williams et al. 2014). While Fig. 2 offers a snapshot of DSD time series measurements, Fig. 3 reveals details of the statistical properties of the DSD spectra in terms of rain rate and D_m.

4. Procedures for evaluation of DPR retrieval uncertainties

An overarching goal of GPM DPR is to obtain three-dimensional rain structures. As such, accurate estimates of rain rate from the DPR are critical to the success of the GPM mission. Because the DPR, operating at Ku and Ka bands, is subject to rain attenuation, accurate attenuation correction is crucial to ensuring the accuracy of rain estimates using dual-wavelength techniques. To assess effectively the uncertainties in the DPR profiling algorithms with respect to DSD parameterizations, comparisons of Ku- and Ka-band specific attenuations, in addition to rain rate, are made between the retrieved and true values. A comparison of D_m is also included because it is one of the important physical

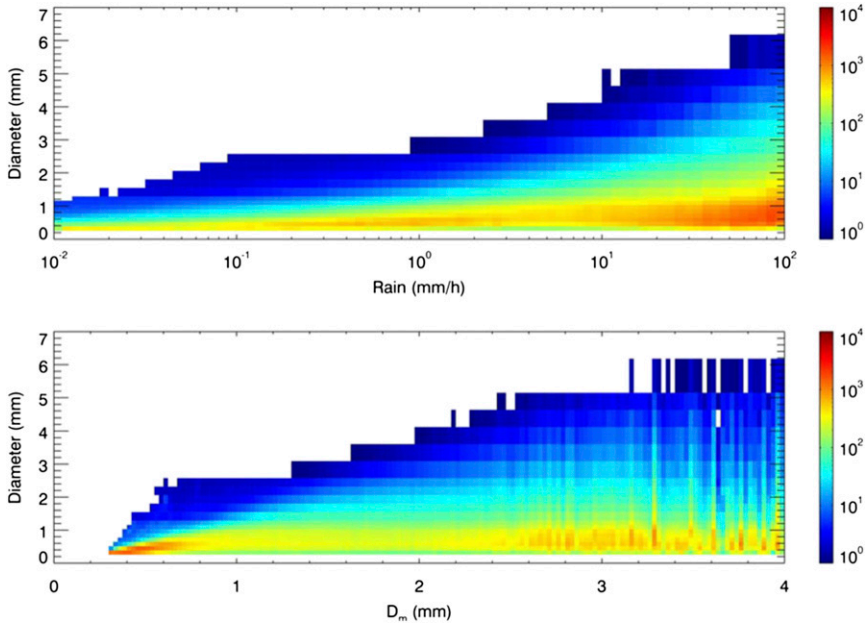

FIG. 3. Mean DSD spectra (color scales) obtained from the full set of measurements of 11 Parsivel disdrometers during IFloodS with respect to (top) rain rate and (bottom) D_m.

parameters of the DSD and can be derived directly from DSD spectra.

A flowchart is shown in Fig. 4 that outlines the procedure used to evaluate DPR estimates by comparing them with the same quantities obtained from measured DSD. As described previously, measured DSD data can be used to compute rain rate and D_m by using Eqs. (7) and (15), respectively. Moreover, specific attenuations can also be derived from the measured DSD by using Eq. (3) and single-particle-scattering tables that provide the extinction cross sections. These results, independent of DSD parameterizations, follow directly from the measured DSD spectra and therefore serve as truth to the radar retrievals. Likewise, the Ku- and Ka-band radar reflectivity factors [Z(Ku) and Z(Ka)], which are generated from the DSD data by using Eq. (2) along with single-particle-scattering tables, are considered to be the true radar reflectivity factors. The simulated

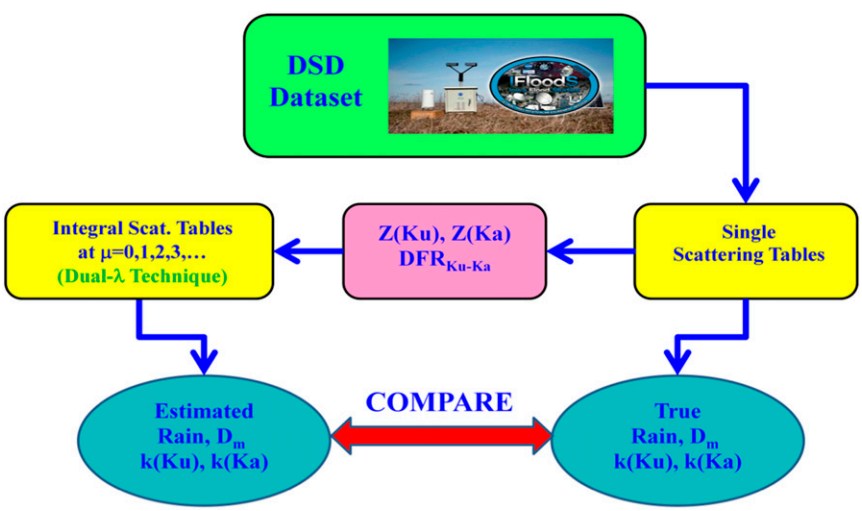

FIG. 4. Flowchart illustrating the procedures for evaluation of the uncertainties in the estimation of rain and attenuation from the dual-wavelength algorithms associated with the choice of DSD model.

Z(Ku) and Z(Ka) are first used to estimate DFR by taking the ratio of Z(Ku) and Z(Ka). Because this ratio is independent of N_w, the DFR yields an estimate of D_m under an assumed shape factor of a gamma DSD distribution. From Z(Ku) and D_m, N_w is subsequently estimated from Eq. (2). Then, Estimates of rain rate and attenuation coefficients are obtained from derived DSD parameters.

Implementation of the dual-wavelength techniques is actually achieved via the integral-scattering tables. As mentioned in section 2, these tables contain precomputed DSD-weighted integral-scattering quantities that are normalized by N_w and indexed with respect to D_m and temperature. Since the integral-scattering tables are DSD-model dependent, each table corresponds to a particular DSD model. In particular, integral-scattering tables prepared for different μ values or for different μ–Λ relations are considered to be different (gamma) DSD models. In fact, estimates of rain rate, D_m, k_{Ku}, and k_{Ka} from the dual-wavelength technique can be viewed as the retrieval results derived from the particular DSD model/table that is used. Thus, comparison of the retrieval results with the truth, obtained directly from the DSD spectra, provide insight as to the accuracy of the DSD model that is employed.

5. Uncertainties of DPR algorithms

As indicated earlier, one of the important objectives of this study is to evaluate the accuracy of the DSD model used in GPM DPR algorithms. The DSD model that the DPR algorithm currently adopts is the gamma distribution with a constant shape factor ($\mu = 3$) (Seto et al. 2013). Note that the same DSD model has been used in the TRMM Precipitation Radar retrieval algorithm (Iguchi et al. 2000). Among the DPR-derived quantities of interest are rain rate, D_m, and specific attenuations that are inferred through the precomputed lookup tables. As noted earlier, the true values of these quantities are those computed directly from the measured DSD spectra. The degree to which the radar estimates agree with these true values serves as an estimate of algorithm accuracy with respect to this error source. Following the procedure shown in Fig. 4, the DPR retrievals are run from the inputs of the simulated Ku- and Ka-band radar reflectivity factors as determined from the measured DSD. Depicted in Fig. 5 are the scatterplots showing comparisons of rain rate, D_m, and specific attenuations between the DPR-retrieved and true values obtained from the spectra of the 11 Parsivel disdrometers. For reference, one-to-one lines (red) are shown on each plot in Fig. 5. For the radar retrieval, the shape parameter μ of the gamma distribution is fixed at 3. Because the DPR Ku-band sensitivity is approximately 17 dBZ, measured DSD data are used only if the corresponding Ku-band radar reflectivity is greater than or equal to 17 dBZ. As noted earlier, D_m has two solutions when DFR is less than 0. This corresponds to values of D_m that are smaller than ~1 mm. In the retrievals used here, the upper branch of the DFR–D_m relations (i.e., the range in which DFR is directly proportional to D_m) is used for the retrieval of D_m. In an attempt to avoid or reduce uncertainties in the D_m dual-value region, a further constraint is added for selection of the DSD data that requires that D_m exceed 1 mm. The total numbers of data points in Fig. 5 that meet these criteria are approximately 50 000, where each point is derived from a minutely averaged drop spectrum. It is found that correlations ρ between the retrieved and true values are in general very high. This result is particularly true for the rain rates and specific attenuations, for which ρ exceeds 0.98. Plots of the data as two-dimensional probability density functions (pdf) of rain rate, D_m, and specific attenuations are given in Fig. 6 using the same data as are shown in Fig. 5. The plots make clear that the majority of data points are near the one-to-one line (solid lines), implying the soundness of the DSD model ($\mu = 3$) that was used for the DPR retrieval.

Comparisons shown in Figs. 5 and 6 are made for a fixed-μ ($\mu = 3$) gamma distribution of DSD model. Similar comparisons can be repeated for different μ values. To quantitatively compare uncertainties in dual-wavelength retrievals from different DSD models, the relative error is used to describe uncertainties in the hydrometeor properties and scattering parameters as derived from the DPR relative to the results computed directly from measured DSD. Let x_{est} and x_{true} represent the radar-estimated and true values, respectively, of rain rate, D_m, k_{Ku}, or k_{Ka}. The bias of x, denoted by $\delta(x)$, is defined as the mean difference of x between estimated and true values within an interval of $(x - \Delta x/2, x + \Delta x/2)$:

$$\delta(x) = \frac{1}{N_x} \sum_{n=1}^{N_x} [x_{\mathrm{est}}(n) - x_{\mathrm{true}}(n)], \tag{16}$$

where N_x is the total number of points in the interval and $x_{\mathrm{est}}(n)$ and $x_{\mathrm{true}}(n)$ are respectively the radar-estimated and true values of x at the nth data point that satisfy

$$|x_{\mathrm{est}} - x| \le \frac{\Delta x}{2}. \tag{17}$$

In light of Eq. (17), the summation in Eq. (16) is carried out only over the data points for which x_{est} is within the interval of $(x - \Delta x/2, x + \Delta x/2)$, where the bin size Δx is set to 2 mm h^{-1}, 0.1 mm, 0.2 dB km^{-1}, and 0.2 dB km^{-1}

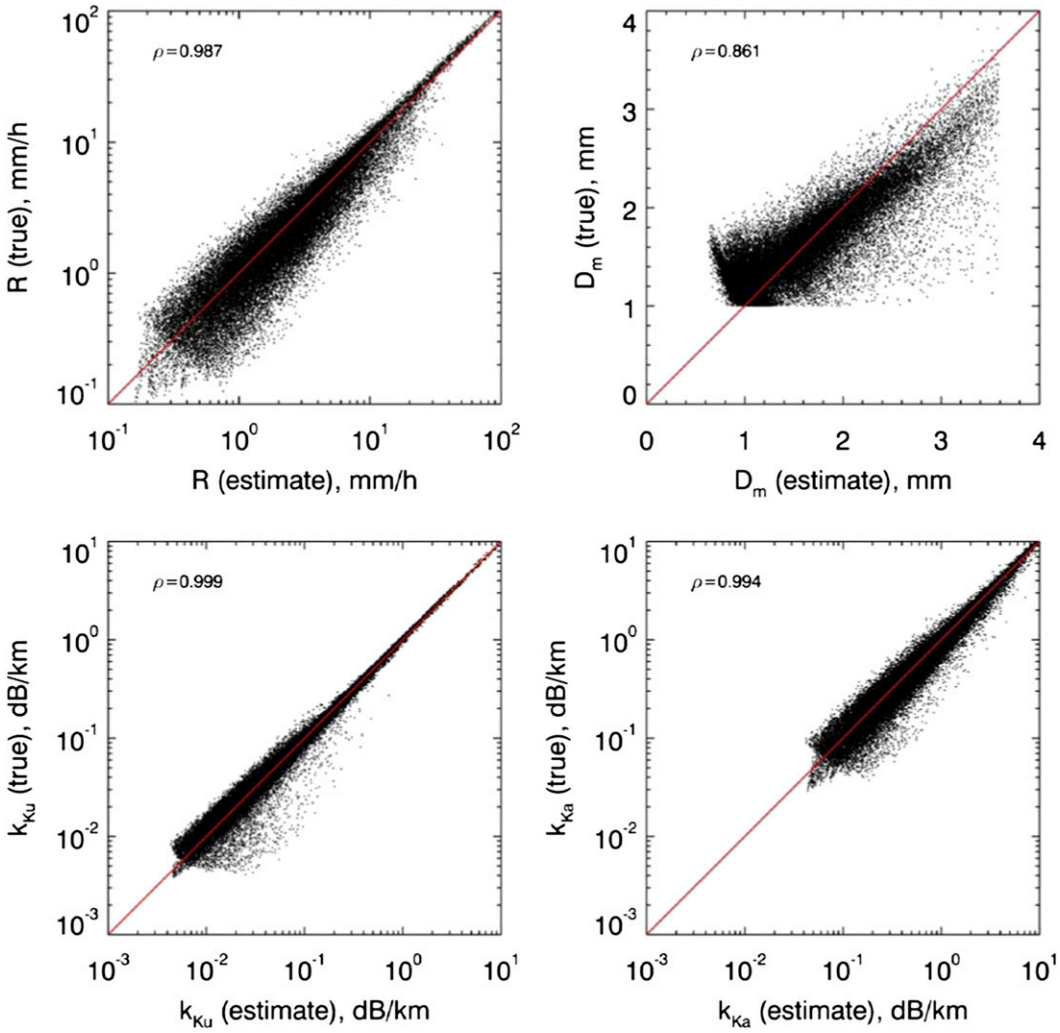

FIG. 5. Comparisons of retrieved rain, D_m, and Ku- and Ka-band specific attenuations (k_{Ku} and k_{Ka}) with their true values that are computed directly from DSD data obtained from 11 Parsivel disdrometers during IFloodS. The correlation coefficient is ρ, and the number of total data points is approximately 50 000.

for rain rate, D_m, k_{Ku}, and k_{Ka}, respectively. The relative bias $\delta_R(x)$ is defined by

$$\delta_R(x) = \delta(x)/x, \tag{18}$$

where $\delta_R(x)$ represents the fractional error of the variable x and is employed to quantify the retrieval accuracy with respect to different DSD parameterizations.

Shown in Fig. 7 are the results of the relative biases of rain rate, D_m, k_{Ku}, and k_{Ka} from DSD gamma distributions with μ equal to 0, 3, 6, and 10. It is evident that the retrieved rain rates at $\mu = 0$ (exponential distribution) are greatly overestimated for rain rates up to 50 mm h^{-1} while the results at $\mu = 6$ show a small underestimation. The DPR-estimated rain rate is within $\pm 10\%$ bias if μ is chosen at 3 or 6. This is true for the results of the Ka-band specific attenuation. The errors in the Ku-band specific attenuation, on the other hand, are generally small and show no significant dependence on μ except for the results associated with DSD exponential distribution ($\mu = 0$). Retrievals of D_m have much larger uncertainties for D_m of less than 1 mm, the case in which D_m has dual values, than those for D_m exceeding 1 mm. This is due to the fact that the DFR is relatively insensitive to D_m when D_m is equal to or less than 1 mm, as shown in Fig. 1. Thus, in this range, a small error in DFR can lead to a large uncertainty in the estimate of D_m. Overall, the estimates from the gamma DSD model with $\mu = 3$ yield the best accuracy, followed by those from $\mu = 6$ and $\mu = 10$. The results of D_m for $\mu = 0$ exhibit large underestimates when D_m is less than 2 mm and overestimates when D_m is greater than 2 mm.

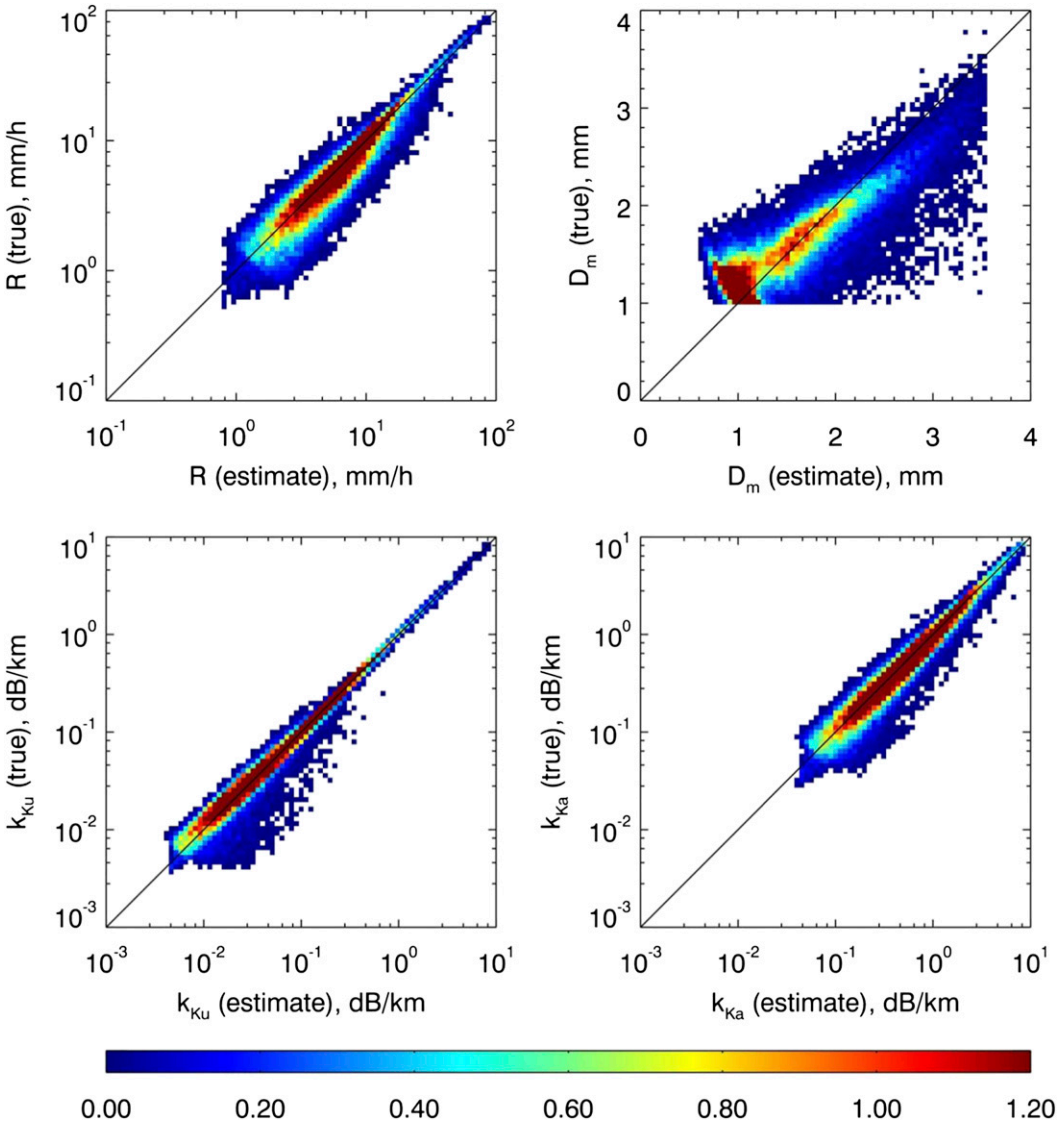

FIG. 6. Two-dimensional pdfs (color scales) that correspond to the data points displayed in Fig. 5.

Analysis of the comparisons in Fig. 7 implies that the gamma DSD parameterizations with fixed μ values that are between 3 and 6 provide consistent and fairly accurate retrievals of rain and Ku- and Ka-band-specific attenuations. Some studies suggest the usefulness of gamma DSD models with μ related to Λ, namely, μ–Λ relations (Zhang et al. 2001; Munchak and Tokay 2008; Kumar et al. 2011; Williams et al. 2014). To evaluate retrieval uncertainties from these constrained models, Fig. 8, similar to Fig. 7, displays the relative biases of the DPR retrievals when the DSD model is replaced by the μ–Λ gamma distributions reported by Zhang et al. (2001), Kumar et al. (2011), and Williams et al. (2014), respectively. The μ–Λ relation found by Zhang et al. (2001) is based on video disdrometer observations in east-central Florida during the summer of 1998, and the relations obtained by Kumar et al. (2011) are derived from Joss–Waldvogel disdrometer measurements made in Singapore from August 1994 to September 1995. Williams et al. (2014) obtained a μ–Λ relation from an analysis of surface disdrometer data and a statistical relationship between DSD spectrum mean diameter and mass spectrum standard deviation. Note that the μ–Λ relations were fitted according to ranges of rain intensities in the Kumar et al. study. The relation used in Fig. 8 from Kumar et al. is for the case in which rain is greater than $1\,\mathrm{mm\,h^{-1}}$. To compare with the fixed-μ gamma models, the results of Fig. 7 for $\mu = 3$ are replotted in Fig. 8. Comparison of the results indicates that the retrieval errors from the μ–Λ relations are generally

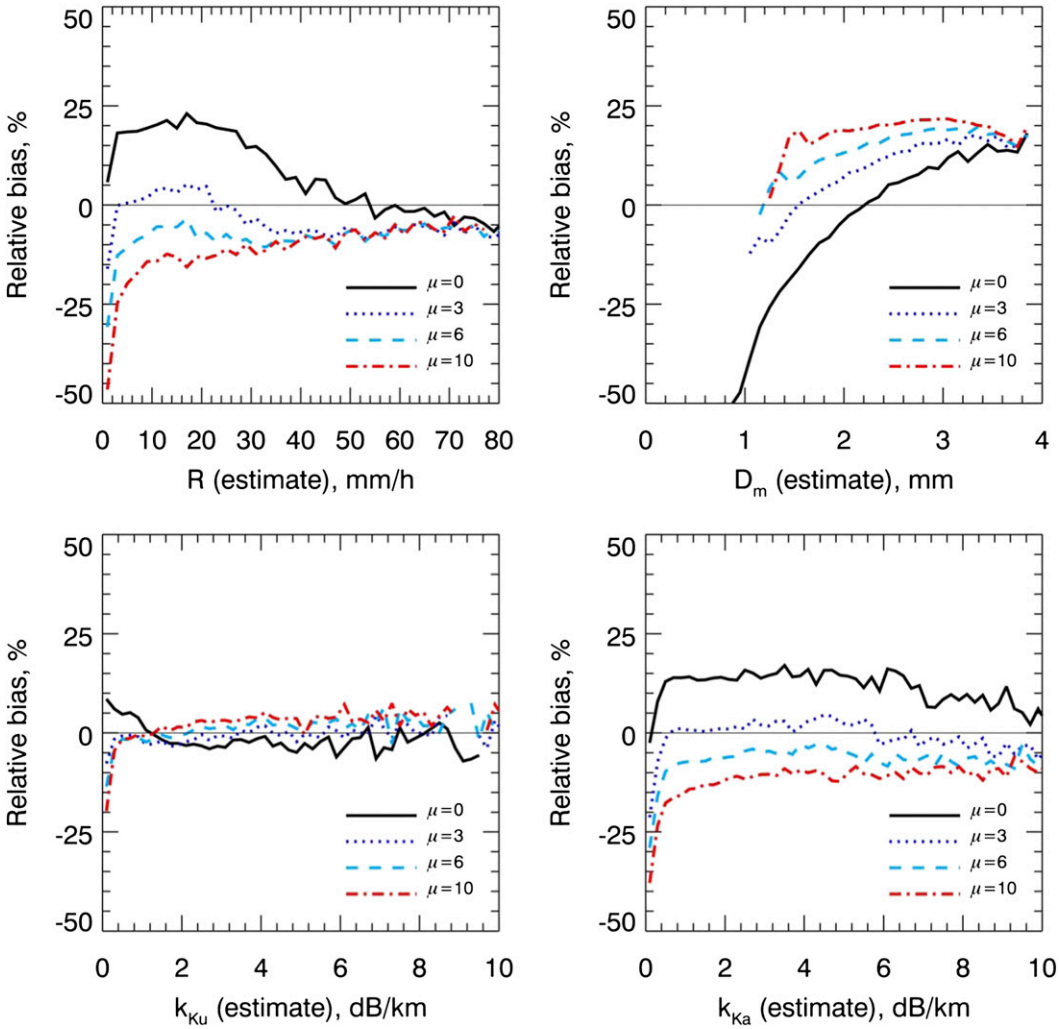

FIG. 7. Relative biases of the DPR-like dual-wavelength retrievals relative to their true values obtained directly from the DSD measurements. A fixed-μ gamma distribution is assumed for the DPR retrieval for μ values of 0, 3, 6, and 10.

small and are comparable to the results from the fixed-μ gamma models with μ equal to 3. The μ–Λ relation proposed by Kumar et al. (2011) seems to provide slightly better accuracy than the others for estimates of rain rate and attenuation.

The lognormal distribution has also been used to describe the rain DSD (Ajayi and Olsen 1985; Feingold and Levin 1986; Maciel and Assis 1990; Tian et al. 2010) and is given by

$$N(D) = \frac{N_t}{\sigma D\sqrt{2\pi}} \exp\left[-\frac{1}{2}\left(\frac{\ln D - \tilde{\mu}}{\sigma}\right)^2\right], \quad (19)$$

where N_t is the number concentration (m^{-3}) and $\tilde{\mu}$ and σ are, respectively, the mean and standard deviation of $\ln D$. Diameter D_m is related to $\tilde{\mu}$ and σ by

$$\ln D_m = \tilde{\mu} + 3.5\sigma^2. \quad (20)$$

One of the important properties of the lognormal distribution is that all of the moments of the distribution are themselves lognormally distributed. To use the lognormal DSD model for dual-wavelength radar retrievals, three parameters of lognormal distribution need to be reduced to two. One possible choice is to fix σ. Williams et al. (2014) have recently developed a relation of DSD mass spectrum standard deviation σ_m and D_m that is based on two-dimensional video disdrometers, which is expressed by

$$\sigma_m = 0.3D_m^{1.36}. \quad (21)$$

The σ_m–D_m constraint described above leads to the following relationships for the lognormal DSD model:

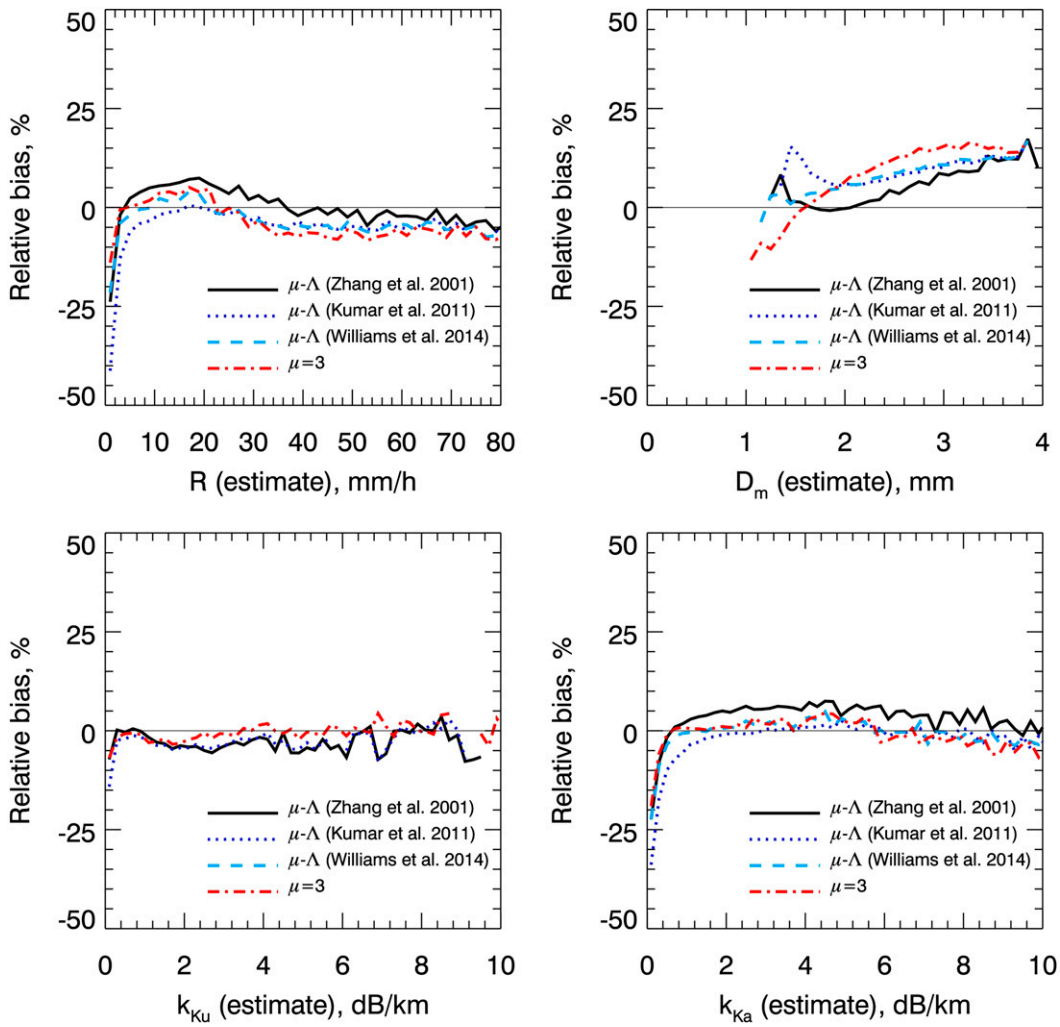

FIG. 8. Relative biases of the DPR-like dual-wavelength retrievals assuming a μ–Λ gamma DSD model relative to the true values obtained directly from DSD measurements. The results from the gamma distribution with fixed-μ value of 3 are plotted for reference.

$$\sigma^2 = \frac{2}{7}(\ln D_m - \tilde{\mu}) \quad \text{and} \tag{22}$$

$$\tilde{\mu} = -3.5\ln(D_m^{-0.286} + 0.09D_m^{0.434}). \tag{23}$$

Equations (22) and (23) imply a relationship between σ and $\tilde{\mu}$. The DSD with such a constraint will be referred to as the $\tilde{\mu}$–σ-constrained lognormal DSD.

Figure 9 displays the relative biases of the estimated parameters to the true values when DSD is modeled as a lognormal distribution with fixed σ values of 0.3, 0.35, and 0.5; also shown are results from the $\tilde{\mu}$–σ-constrained relation given by Eqs. (22) and (23). Of these models, the lognormal DSD with $\sigma = 0.35$ and the constrained $\tilde{\mu}$–σ relation apparently yield the best agreement in rain rate and attenuation coefficient despite the fact that all of them are somewhat biased in estimates of D_m. As shown in Fig. 9, the results derived from the lognormal distribution with $\sigma = 0.35$ and a lognormal distribution using a $\tilde{\mu}$–σ relation yield nearly identical error statistics.

6. Summary

A framework has been developed for an assessment of the accuracy and uncertainties of DSD models employed in dual-wavelength radar retrievals. The principle of our approach is based on measured DSD data, from which GPM DPR reflectivity signatures are generated through use of single-scattering tables. The simulated Ku- and Ka-band radar reflectivity factors are considered as DPR measurements and are used as inputs to a dual-frequency radar technique, using the DPR frequencies, for the

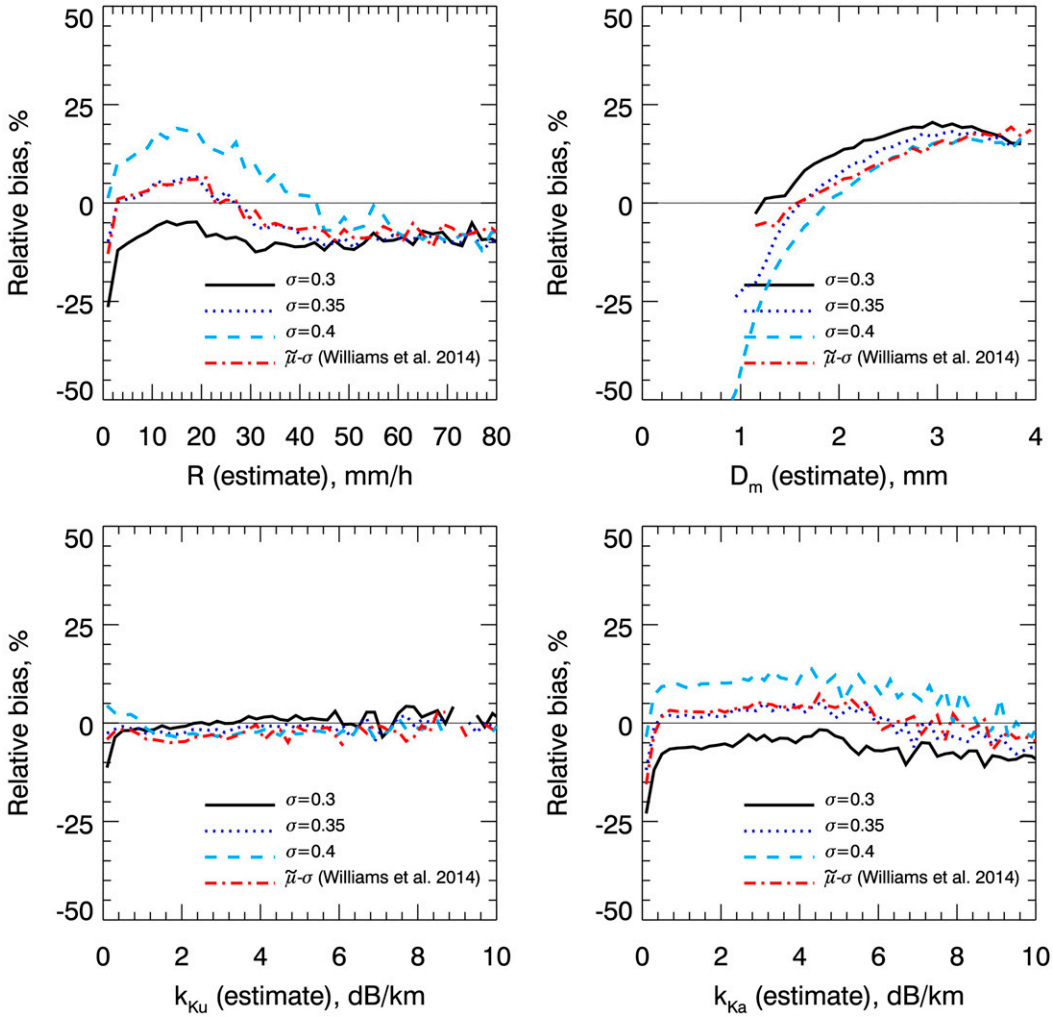

FIG. 9. Relative biases of the DPR-like dual-wavelength retrievals when a lognormal DSD model is used. The results from three fixed-σ values of 0.3, 0.35, and 0.4, as well as results that are based on a $\tilde{\mu}$–σ relation inferred from Williams et al. (2014), are shown.

retrieval of D_m and N_w. The rain rates, D_m, and specific attenuations obtained from the measured size distributions are compared with the same quantities computed directly from the data so that the accuracy of DPR algorithms with respect to the DSD parameterization can be evaluated. Comparisons of the relative biases of the DPR-retrieved rain and attenuation coefficients among different DSD models provide an effective means to identify appropriate DSD models to be used in the dual-wavelength radar retrieval of rain profiles.

A large set of DSD measurement data (approximately 50 000 minutely averaged spectra), taken from 11 Parsivel disdrometers during the IFloodS field campaign, are employed in this study for assessment of retrieval uncertainties in connection with the choice of DSD model within the context of dual-frequency retrievals. Two types of the gamma distribution, one with fixed μ and another using a μ–Λ relation, are examined. Analysis of the comparisons of different DSD models reveals that dual-wavelength retrievals using the fixed-μ gamma distributions with μ ranging from 3 to 6 as well as the μ–Λ relations generally yield the smallest error. It is anticipated that the DPR at-launch algorithms that use the fixed-μ (μ = 3) gamma distribution will provide fairly accurate and consistent estimates of rain rate and attenuation.

Note that the framework described in this study for evaluation of DSD models is distinct from studies that concentrate on modeling DSD spectra, such as the work reported by Williams et al. (2014). The approach here is algorithm dependent and selects those DSD models that

best represent the DFR and other radar-measured quantities, whereas the goal of the latter type of approach is to determine how best to model the measured spectra from a mathematical and physical perspective using parameterizations that are independent of a particular algorithm or radar measurement. Note also that the choice of DSD model is just one of many issues in the DPR profiling algorithm that include, but are not limited to, path attenuation, hydrometeor particle scattering, storm classification, phase identification, environment assumptions, and nonuniform beam filling. Success of the DPR algorithm will depend not only on the accuracy of each of these modules but on their integrated performance.

Although the procedures described in this study are aimed at evaluation of uncertainties for Ku- and Ka-band dual-wavelength radar, the method should be applicable to polarimetric measurements or different combinations of radar frequencies including single-, dual-, or triple-frequency radar and possibly radar–radiometer combined algorithms. Because the DSD data used in this study were collected in Iowa during the summer, our findings might not be representative of other climatological behavior. In future studies we hope to apply the approach to different DSD models and to DSD datasets representing different climatological regimes.

Acknowledgments. This work is supported by Dr. R. Kakar of NASA Headquarters under NASA's Precipitation Measurement Mission (PMM) Grant NNH12ZDA001N-PMM. The authors also thank the IFloodS Science Team for providing Parsivel disdrometer data.

REFERENCES

Ajayi, G. O., and R. L. Olsen, 1985: Modeling of a tropical raindrop size distribution for microwave and millimeter wave applications. *Radio Sci.,* **20,** 193–202, doi:10.1029/RS020i002p00193.

Battan, L. J., 1973: *Radar Observation of the Atmosphere.* University of Chicago Press, 324 pp.

Bringi, V. N., and V. Chandrasekar, 2001: *Polarimetric Doppler Weather Radar—Principles and Applications.* Cambridge University Press, 664 pp.

——, G. Huang, V. Chandrasekar, and E. Gorgucci, 2002: A methodology for estimating the parameters of a gamma raindrop size distribution model from polarimetric radar data: Application to a squall-line event from the TRMM/Brazil campaign. *J. Oceanic Atmos. Technol.,* **19,** 633–645, doi:10.1175/1520-0426(2002)019<0633:AMFETP>2.0.CO;2.

Feingold, G., and Z. Levin, 1986: The lognormal fit to raindrop spectra from frontal convective clouds in Israel. *J. Appl. Meteor.,* **25,** 1346–1363, doi:10.1175/1520-0450(1986)025<1346:TLFTRS>2.0.CO;2.

Gorgucci, E., G. Scarchilli, V. Chandrasekar, and V. N. Bringi, 2000: Measurement of mean raindrop shape from polarimetric radar observations. *J. Atmos. Sci.,* **57,** 3406–3413, doi:10.1175/1520-0469(2000)057<3406:MOMRSF>2.0.CO;2.

——, ——, ——, and ——, 2002: Estimation of raindrop size distribution parameters from polarimetric radar measurements. *J. Atmos. Sci.,* **59,** 2373–2384, doi:10.1175/1520-0469(2002)059<2373:EORSDP>2.0.CO;2.

Hou, A., G. S. Jackson, C. Kummerow, and C. M. Shepherd, 2008: Global precipitation measurement. *Precipitation: Advances in Measurement, Estimation, and Prediction,* S. Michaelides, Ed., Springer, 131–169.

Iguchi, T., T. Kozu, R. Meneghini, J. Awaka, and K. Okamoto, 2000: Rain-profiling algorithm for the TRMM Precipitation Radar. *J. Appl. Meteor.,* **39,** 2038–2052, doi:10.1175/1520-0450(2001)040<2038:RPAFTT>2.0.CO;2.

Kumar, L. S., Y. H. Lee, and J. T. Ong, 2011: Two-parameter gamma drop size distribution models for Singapore. *IEEE Trans. Geosci. Remote Sens.,* **49,** 3371–3380, doi:10.1109/TGRS.2011.2124464.

Liao, L., and R. Meneghini, 2005: A study of air/space-borne dual-wavelength radar for estimates of rain profiles. *Adv. Atmos. Sci.,* **22,** 841–851, doi:10.1007/BF02918684.

Maciel, L. R., and M. Assis, 1990: Tropical rainfall drop-size distribution. *Int. J. Satell. Commun.,* **8,** 181–186, doi:10.1002/sat.4600080310.

Mardiana, R., T. Iguchi, and N. Takahashi, 2004: A dual-frequency rain profiling method without the use of a surface reference technique. *IEEE Trans. Geosci. Remote Sens.,* **42,** 2214–2225, doi:10.1109/TGRS.2004.834647.

Meneghini, R., and L. Liao, 2013: Modified Hitschfeld–Bordan equations for attenuation-corrected radar rain reflectivity: Application to nonuniform beamfilling at off-nadir incidence. *J. Atmos. Oceanic Technol.,* **30,** 1149–1160, doi:10.1175/JTECH-D-12-00192.1.

——, H. Kumagai, J. R. Wang, T. Iguchi, and T. Kozu, 1997: Microphysical retrievals over stratiform rain using measurements from an airborne dual-wavelength radar radiometer. *IEEE Trans. Geosci. Remote Sens.,* **35,** 487–506, doi:10.1109/36.581956.

Mishchenko, M. I., and L. D. Travis, 1998: Capabilities and limitations of a current FORTRAN implementation of the T-matrix method for randomly oriented, rotation symmetric scatterers. *J. Quant. Spectrosc. Radiat. Transfer,* **60,** 309–324, doi:10.1016/S0022-4073(98)00008-9.

Munchak, S. J., and A. Tokay, 2008: Retrieval of raindrop size distribution from simulated dual-frequency radar measurements. *J. Appl. Meteor. Climatol.,* **47,** 223–239, doi:10.1175/2007JAMC1524.1.

Rose, C. R., and V. Chandrasekar, 2005: A system approach to GPM dual-frequency retrieval. *IEEE Trans. Geosci. Remote Sens.,* **43,** 1816–1826, doi:10.1109/TGRS.2005.851165.

Schönhuber, M., G. Lammer, and W. L. Randeu, 2007: One decade of imaging precipitation measurement by 2D-video-disdrometer. *Adv. Geosci.,* **10,** 85–90, doi:10.5194/adgeo-10-85-2007.

Seto, S., T. Iguchi, and T. Oki, 2013: The basic performance of a precipitation retrieval algorithm for the Global Precipitation Measurement mission's single/dual-frequency radar measurements. *IEEE Trans. Geosci. Remote Sens.,* **51,** 5239–5251, doi:10.1109/TGRS.2012.2231686.

Smith, P. L., D. V. Kliche, and R. W. Johnson, 2009: The bias and error in moment estimators for parameters of drop size distribution functions: Sampling from gamma distributions. *J. Appl. Meteor. Climatol.,* **48,** 2118–2126, doi:10.1175/2009JAMC2114.1.

Thurai, M., G. J. Huang, V. N. Bringi, W. L. Randeu, and M. Schönhuber, 2007: Drop shapes, model comparisons, and calculations of polarimetric radar parameters in rain. *J. Atmos. Oceanic Technol.,* **24,** 1019–1032, doi:10.1175/JTECH2051.1.

——, W. A. Petersen, A. Tokay, C. Schultz, and P. Gatlin, 2011: Drop size distribution comparisons between Parsivel and 2-D video disdrometers. *Adv. Geosci.,* **30,** 3–9, doi:10.5194/adgeo-30-3-2011.

Tian, L., G. M. Heymsfield, A. J. Heymsfield, A. Bansemer, L. Li, C. H. Twohy, and R. C. Srivastava, 2010: A study of cirrus ice particle size distribution using TC4 observations. *J. Atmos. Sci.,* **67,** 195–216, doi:10.1175/2009JAS3114.1.

Tokay, A., W. A. Petersen, P. Gatlin, and M. Wingo, 2013: Comparison of raindrop size distribution measurements by collocated disdrometers. *J. Atmos. Oceanic Technol.,* **30,** 1672–1690, doi:10.1175/JTECH-D-12-00163.1.

——, D. B. Wolff, and W. A. Petersen, 2014: Evaluation of the new version of laser-optical disdrometer, OTT Parsivel^2. *J. Atmos. Oceanic Technol.,* **31,** 1276–1288, doi:10.1175/JTECH-D-13-00174.1.

Ulbrich, C. W., 1983: Natural variations in the analytical form of the raindrop size distribution. *J. Climate Appl. Meteor.,* **22,** 1764–1775, doi:10.1175/1520-0450(1983)022<1764:NVITAF>2.0.CO;2.

Williams, C., and Coauthors, 2014: Describing the shape of raindrop size distributions using uncorrelated raindrop mass spectrum parameters. *J. Appl. Meteor. Climatol.,* **53,** 1282–1296, doi:10.1175/JAMC-D-13-076.1.

Zhang, G., J. Vivekanandan, and E. Brandes, 2001: A method for estimating rain rate and drop size distribution from polarimetric radar. *IEEE Trans. Geosci. Remote Sens.,* **39,** 830–840, doi:10.1109/36.917906.